Engineering Fracture Mechanics 111 (2013) 50–64

Contents lists available at ScienceDirect

Engineering Fracture Mechanics

journal homepage: www.elsevier.com/locate/engfracmech

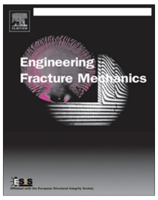

Mixed mode (I + II) fracture toughness of polymer nanoclay nanocomposites

Michele Zappalorto, Marco Salviato, Marino Quaresimin [*]

Department of Management and Engineering, University of Padova, Stradella San Nicola 3, 36100 Vicenza, Italy

ARTICLE INFO

Article history:
Received 3 May 2013
Received in revised form 8 August 2013
Accepted 17 September 2013
Available online 25 September 2013

Keywords:
Nanocomposites
Nanoclay
Fracture toughness
Mixed mode fracture

ABSTRACT

In this work the mixed mode fracture behaviour (I + II) of an epoxy/nanoclay nanocomposite system is analysed, discussing the results from Single Edge Notch Bending tests. It is found that nanomodification significantly enhances the fracture toughness of the epoxy resin on the entire range of mixed mode loadings (from pure mode I to pure mode II), improvements depend however on the mode mixity.

Experimental results are compared to theoretical predictions based on different criteria for mixed mode fracture in brittle homogeneous materials. As expected, it is found that, while the data from pure epoxy are satisfactorily predicted almost independently of the adopted approach, the agreement is much worse in the case of nanomodified materials. Explanations of this behaviour can be found in the emergence of additional microscale and nanoscale toughening mechanisms due to nanomodification not properly described by conventional models.

1. Introduction

Nanotechnology is a rapidly emerging technology with great potential to create new multifunctional materials, characterised by enhanced physical and mechanical properties and new improved products for numerous fields of application [1–3].

The most interesting aspect related to nanomodified polymers is that, different from traditional fibre reinforced composites, they are endowed with exceptionally improved properties at very low filler concentrations. The explanation of this peculiar phenomenon, often regarded as "nano-effect", can be sought in the interactions at the atomic scale. Indeed as the filler size is decreased to the nanoscale, the specific surface area rapidly increases, making surface properties the dominant factor and providing unique properties with widespread applications in many industrial sectors. Moreover, as the reinforcement size is comparable with that of polymeric chains, molecular interactions with the matrix produce an interphase "layer", whose properties can differ substantially from those of the constituents. The properties of this interphase zone play a very important role in the amount of energy dissipated by the different damaging mechanisms taking place at the nano-scale and, in turn, on the overall mechanical properties of the nanocomposite, depending also on the filler size and geometry [4–7].

Also nanofiller morphology can play an important role. Dealing with the filler morphology, main differences are essentially due to the nanofiller typology, which might be distinguished in nanoclays, nanoparticles and nanotubes. In particular clay based nanocomposites have revealed to be a very promising technology in the perspective of achieving high performances at a relative low cost.

---

[*] Corresponding author.
E-mail address: marino.quaresimin@unipd.it (M. Quaresimin).

0013-7944/$ - see front matter © 2013 Elsevier Ltd. All rights reserved.
http://dx.doi.org/10.1016/j.engfracmech.2013.09.006

Nomenclature

a	crack length
B	specimen thickness
E	tensile elastic modulus
F	applied force
K_{I}, K_{II}	mode I and mode II stress intensity factors
K_{Ic}, K_{IIc}	fracture toughness under pure mode I and pure mode II
L_1, L_2, L_3, L_4	distances between loads and crack plane
M	bending moment at the crack plane
P_{cr}	critical load at fracture
Q	shear force at the crack plane
W	specimen ligament
wt%	weight percent (%) of nanofiller
α_1, and α_2	non-dimensional shape factor
ε_f	strain to failure (%)
ϕ	mode mixity, $K_{\mathrm{II}}/K_{\mathrm{I}}$
ν	Poisson's ratio
θ_0	fracture angle
σ_R	tensile strength
$\sigma_{\theta\theta}$	tangential stress

Nanoclays are layered silicates of which the platelets are micro-sized in area, about 1 nm thick and disposed in stacks called tactoids. Once dispersed in the polymeric matrix three typical nanoclay morphologies are possible, namely, exfoliated, intercalated and phase separated clays. In more details:

- The separated morphology is obtained when the polymer is unable to intercalate between the silicate sheets.
- The intercalated morphology is obtained when one or more extended polymer chain is intercalated between the silicate layers resulting in a well ordered multilayer morphology built up with alternating polymeric and inorganic layers.
- The fully exfoliated morphology is obtained when the silicate layers lose their parallelism and they are completely and uniformly dispersed in a continuous polymer matrix.

With the aim to maximize the "nano-effect", complete exfoliation is highly desirable but it is far from easy to be obtained since it requires the separation of the tactoids from the primary particle, followed by the destruction of the order of the clay platelets within the tactoids. However a balance between an exfoliated and intercalated structure is often sufficient to obtained the desired property enhancements [8–15]. Polymer–nanoclay nanocomposites offer exceptional performances, when compared to those of the neat polymer, in terms of flammability, barrier and mechanical properties. In particular, due to their very high aspect ratio, nanoclay platelets are suitable to improve the tensile elastic modulus of polymeric systems (see [8–10]). On the contrary, conflicting results have been reported with reference to the strength of nanoclay reinforced resins, which has been proven either to increase [11,12] or decrease [12–15], depending on the studied system. The fracture toughness of nanomodified polymers is acknowledged to be the most important mechanical property to be studied, mainly in the perspective they are used as toughened matrixes in ternary, fibre reinforced, nanocomposites [15,16]. This does explain the large attention recently paid by several researchers to the study of the fracture toughness of binary nanocomposites (polymer matrix plus nanofillers) [15,17–22].

Although in practice the stress state ahead of a crack is often of the mixed type, in the best of authors' knowledge all the previous studies dealing with the toughness of nanoclay nanocomposites are limited to pure mode I fracture, whilst extending the analysis to other nanofillers, the only exception seems to be a recent contribution by Ayatollahi et al. for carbon nanotube nanocomposite [23].

With the aim to fill this gap, in this study the mixed mode fracture behaviour of an epoxy resin filled with montmorillonite nanoclays is analysed. After a preliminary investigation on tensile properties, the fracture behaviour of the nanocomposite system is studied and discussed in detail by taking advantage of the results from Single Edge Notch Bending (SENB) tests, considering four loading conditions, ranging from pure mode I to pure mode II. The effect of the mode mixity on the crack paths, fracture toughness improvements and fracture surface morphology are discussed in details as well.

Experimental results are eventually compared to the predictions based on some classical mixed mode fracture criteria (MTS criterion, S criterion, Richard's crietrion), discussing their degree of accuracy.

2. Materials and specimens used in the experimental analysis

In this study, a DGEBA-based epoxy resin (EC157 with W152LR hardener) from Elantas-Camattini was chosen as polymer matrix. The main mechanical properties of the adopted epoxy system, as specified by the supplier, are summarised in Table 1.

Table 1
Properties of EC157/W131 epoxy system as provided by Elantas-Camattini.

E	3.2–3.5 GPa
σ_r	68–76 MPa
ε_r	6–8%

In addition, a montmorillonite clay, Cloisite 30B® from Southern Clay Products, was used as nanosized reinforcement. 30B nanoclays are characterised by 1 nm thick lamellae, lateral dimensions from 70 to 150 nm and average *d*-spacing of about 18.5 Å.

Dog bone (DB) specimens as well as Single Edge Notch Bending (SENB) specimens (Fig. 1) have been produced. SENB specimen dimensions strictly conform to the guidelines of Ref. [24].

The specimens were manufactured according to the following steps:

1. *Dispersion of the filler within the resin.* Initially, in order to get an as good as possible dispersion and distribution of the filler, nanoclays were dispersed within the polymer resin through shear mixing followed by sonication. The shear mixing process was carried out with a DISPERMAT TU shear blender from VMA-Getzmann, at an average rate of 2000 rpm for about 1 h. The sonication process, instead, was performed using a HIELSCHER UP 200s Sonicator, set on 140 W (70% of the maximum power) and a duty cycle of 50%, for 10 min. After sonication, the hardener was added and the obtained blend was mixed at low rate (1000 rpm) for further 5 min.
2. *Degassing and moulding of the obtained blend.* As a major drawback of the shear mixing process, a large amount of air is trapped in the matrix. Thus, in order to prevent void traps and bubbles in the specimens, a degassing process was carried out at room temperature. To this end, a low-vacuum pump was used to induce a very low pressure in the resin pot, promoting bubbles explosion. One hour of degassing process was enough to obtain a clear and translucent nanomodified resin which was later slowly poured into silicone rubber moulds, allowing us to obtain specimens without voids. The different stages of the degassing process are shown in Fig. 2.
3. *Milling and surface polishing.* Samples were then cured at room temperature for about 72 h. Once de-moulded, the specimens were surface milled and polished up to the final thickness.

As far as the SENB specimens are concerned, a further manufacturing step was carried out:

4. *Manual tapping and fatigue propagation up to a 10 mm long crack.* Using a razor blade, the samples were pre-cracked by manual tapping. Finally, 10 mm long cracks (half the specimen width, according to [24]) were obtained from the artificial short cracks after some zero-to-tension fatigue cycles.

The morphology of the materials used in the present analyses has been investigated using Scanning Electron Microscopy, in order to identify the presence of nanofiller agglomerates. Fig. 3 reports some SEM images for 1, 3 and 5 wt% loaded resins. At 1 wt% some traces of clay agglomeration are present (size about 20 μm). For higher contents the dimensions of the

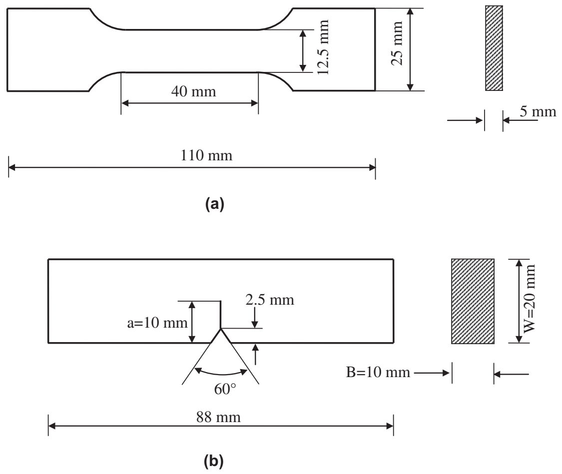

Fig. 1. Dog Bone (DB) specimens (a) and Single Edge Notch Bending (SENB) specimens (b) used in the tests.

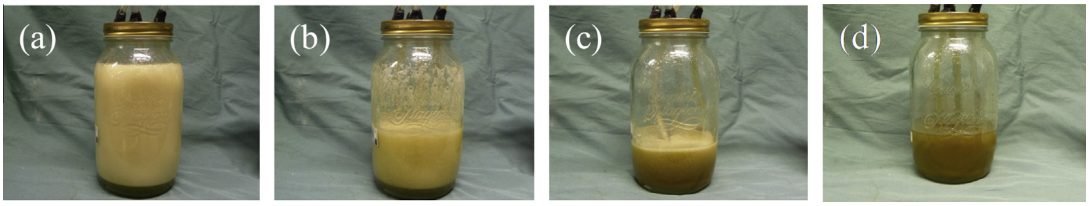

Fig. 2. Degassing process of the nanomodified resin (5 wt% of nanoclay). (a) Nanomodified resin at low pressure as just poured into the pot; (b) after 10 min; (c) after 25 min and (d) after 35 min. At the end of the process, the mixture is devoid of any bubble.

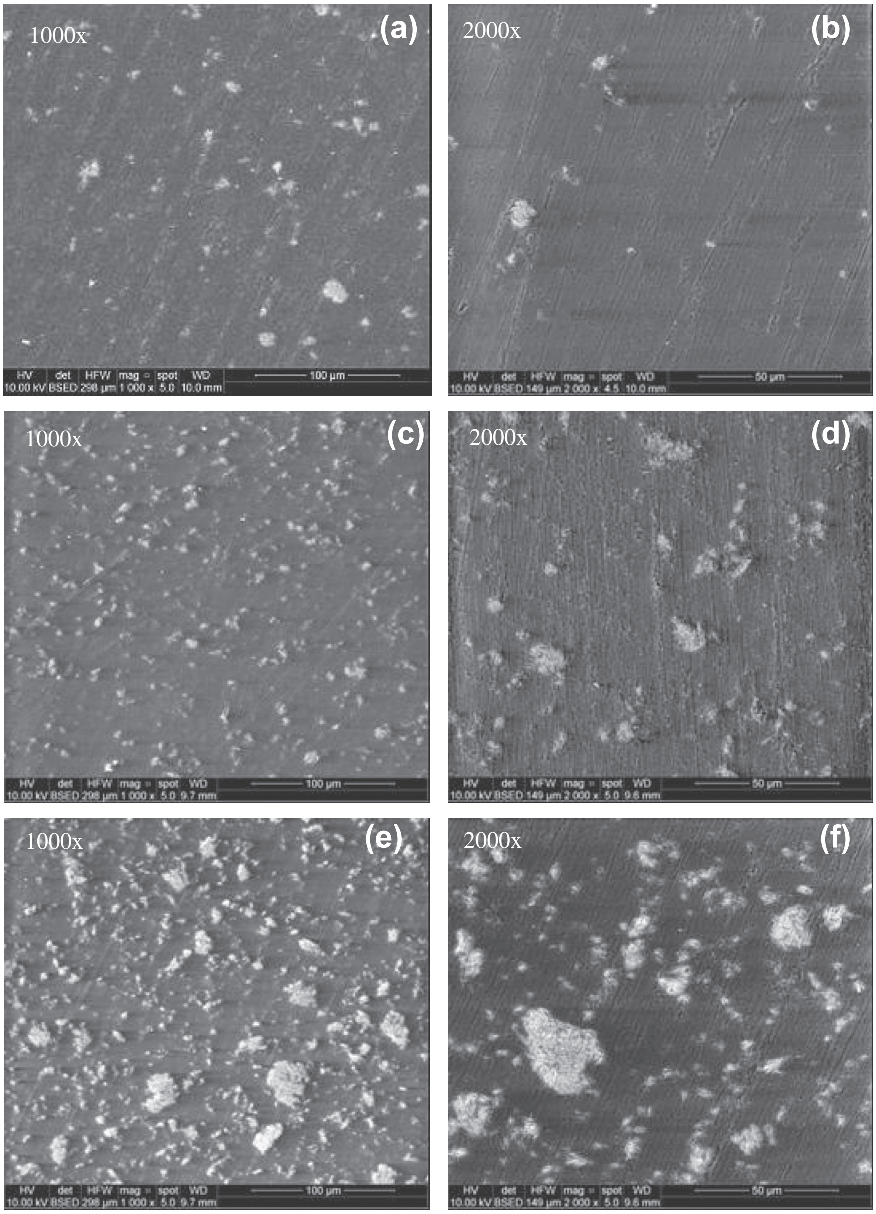

Fig. 3. Morphology of 1 wt% (a and b) 3 wt% (c and d) and 5 wt% (e and f) clay-loaded resins. Scanning electron micrographs at different magnifications.

agglomerates is almost comparable to the ones reported for 1 wt% even if their content is more elevated. However, as a general trend for all the clay contents under investigation, the nanofiller seems to be well distributed within the matrix. Similar morphologies have been found in previous experimental investigations by the present authors [15].

3. Experimental equipment and tests

All tests have been carried out by using a MTS 858 servo-hydraulic machine, equipped with a 2.5/25 kN load cell.

3.1. Tensile tests

Tensile tests on dog-bone specimens with the geometry shown in Fig. 1a, were carried out with the aim to determine the failure stress, σ_R, the elastic modulus, E, the Poisson ratio, ν, and the strain to failure, ε_f of the neat epoxy and nanomodified resins, by using a crosshead speed equal to 2 mm/min. A MTS 632.29F-30 extensometer was used for accurate strain measurements. For each material configuration, at least three specimens were tested. In all the performed tests failure took place in the gauge length of the specimen.

3.2. Single Edge Notch Bending tests

As far as SENB tests are concerned, different loading conditions have been applied, resulting in different mixed mode loadings, which ranged from pure mode I to pure mode II.

The fracture tests have been carried out using a crosshead speed equal to 10 mm/min, as suggested in [24]. At least three specimens for every loading condition and every filler weight fraction were tested.

SENB specimen dimensions and geometry strictly conform to the suggestions reported in Ref. [24], namely $B = 10$ mm, $W = 20$ mm, specimen's length equal to 88 mm (see Fig. 1b).

The testing device consisted of two steel plates, 18 mm thick, one fixed on the load cell, the other attached to a vertical moving ram. One or two pin supports could be mounted on each plate. Some pictures of the loading system are shown in Fig. 4.

3.2.1. Mode I loading tests

The mode I fracture toughness was evaluated using three-point bending tests according to the ASTM-D5045-99 standard [24] (see Fig. 4a). Mode I fracture toughness can be computed from the following expression [24]:

$$K_{\mathrm{Ic}} = \frac{P_{cr}}{BW^{0.5}} f\left(\frac{a}{W}\right) \tag{1}$$

where P_{cr} is the critical load while B, a and W are defined in Fig. 1b. The suggested expression for $f(a/W)$ is [24]:

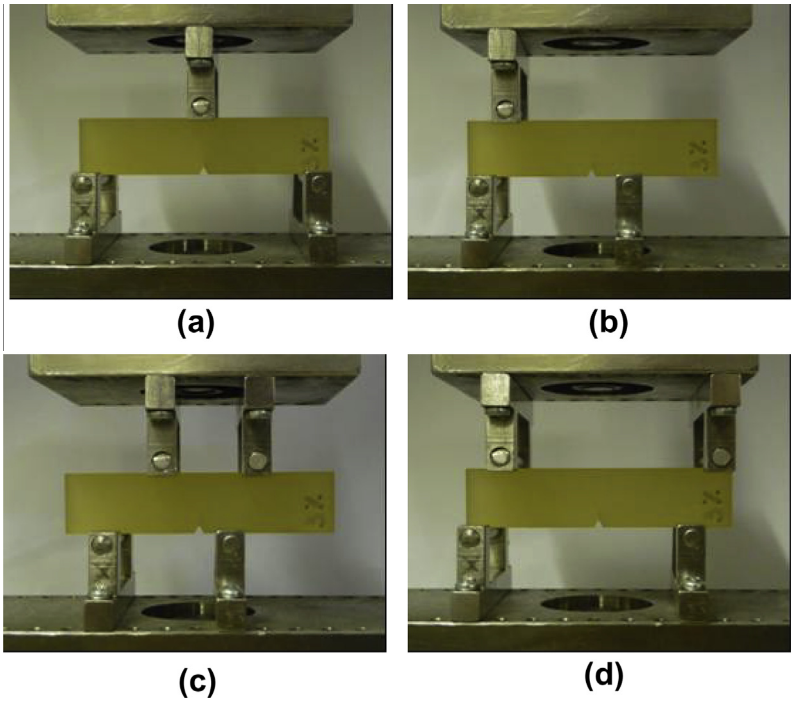

Fig. 4. Loading configurations for pure mode I tests (a), non-Symmetric three Point Bending (NS3PB) tests with $\phi = 0.3$ (b), non-Symmetric four Point Bending (NS4PB) tests with $\phi = 1.35$ (c), non-Symmetric four Point Bending (NS4PB) for pure mode II tests (d).

$$f\left(\frac{a}{W}\right)=6\left(\frac{a}{W}\right)^{0.5}\frac{\left[1.99-\frac{a}{W}\left(1-\frac{a}{W}\right)\left(2.15-3.93\frac{a}{W}+2.7\left(\frac{a}{W}\right)^{2}\right)\right]}{\left(1+2\frac{a}{W}\right)\left(1-\frac{a}{W}\right)^{1.5}}\quad 0<\frac{a}{W}<1 \tag{2}$$

3.2.2. Mixed mode and pure mode II loadings tests

In the best of authors' knowledge no standardized procedures are available for mixed mode or pure mode II fracture testing. Accordingly, the same specimen size and geometry suggested for mode I loading tests [24] have been used, while variations of mode mixity have been obtained changing the loading conditions, using non-symmetric three- and four-point bending configurations. This allowed to broaden out the range of possible loading conditions.

Besides mode I, the following fracture tests have been carried out:

1. Fracture tests under prevalent mode I loading conditions, $\phi = K_{II}/K_I \cong 0.3$. These tests have been carried out using the non-Symmetric three Point Bending (NS3PB) configuration sketched in Fig. 5a and depicted in Fig. 4b;
2. Fracture tests under prevalent mode II loading conditions, $\phi = K_{II}/K_I \cong 1.35$ and under pure mode II loading conditions. These tests have been carried out using the non-symmetric four point bending (NS4PB) configuration sketched in Fig. 5b and depicted in Fig. 4c and d.

Details of loading conditions for mixed mode tests are given in Table 2.

In all cases the crack tip stress intensity factors have been evaluated as:

$$K_I = \sigma_{ng}\alpha_1(a/W)\sqrt{\pi a}\quad K_{II} = \tau_{ng}\alpha_2(a/W)\sqrt{\pi a} \tag{3}$$

where σ_{ng} and τ_{ng} are the maximum nominal stresses on the gross section, evaluated according to the following expressions:

$$\sigma_{ng}=\frac{6M}{BW^2}\quad \tau_{ng}=\frac{3}{2}\frac{Q}{BW} \tag{4a-b}$$

In Eq. (4a) and (4b) M and Q are the bending moment and the shear force evaluated on the crack plane resulting from static equilibrium equations. Accordingly:

$$M = F\frac{L_3-L_1}{L_3+L_4}L_4\quad Q = F\frac{L_3-L_1}{L_3+L_4} \tag{5}$$

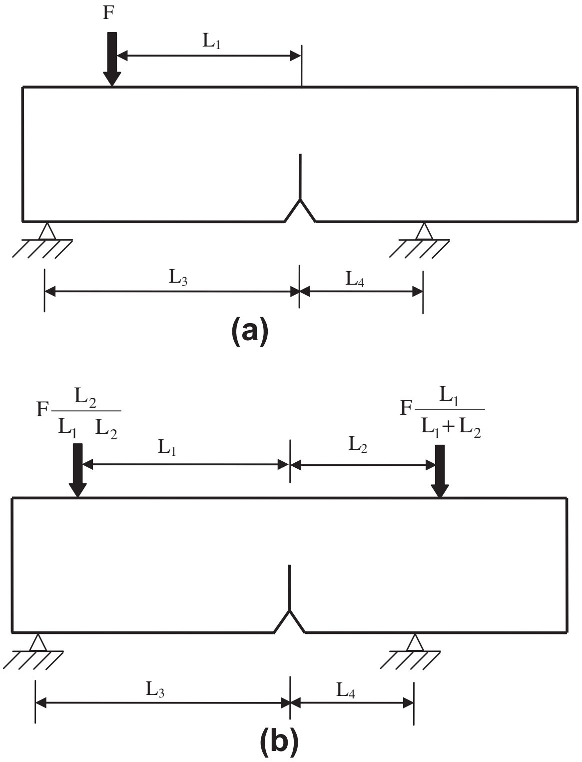

Fig. 5. Schematic of the non-Symmetric three Point Bending (NS3PB) (a) and of the non-Symmetric four Point Bending (NS4PB) (b) loading configurations.

Table 2
Details of loading conditions for mixed mode tests.

Mode mixity K_{II}/K_I	Loading condition	L_1 (mm)	L_2 (mm)	L_3 (mm)	L_4 (mm)
0.3	NS3PB	30	/	40	10
1.35	NS4PB	10	20	30	10
∝	NS4PB	30	40	40	30

for non-symmetric three point bending (Fig. 5a) and:

$$M = F\left(\frac{L_1 L_2}{L_1 + L_2} - \frac{L_3 L_4}{L_3 + L_4}\right) \quad Q = F\left(\frac{L_1}{L_1 + L_2} - \frac{L_3}{L_3 + L_4}\right) \tag{6}$$

for non-symmetric four point bending (Fig. 5b) where F is the total applied load.

Shape functions α_1 and α_2 to be used have been evaluated by means of some finite element analyses and were found to be for, $a/W = 0.5$ (which was used for all specimens in the fracture tests):

$$\alpha_1 = \frac{443}{295} \quad \alpha_2 = \frac{97}{106} \tag{7}$$

for NS3PB (Fig. 5a) and:

$$\alpha_1 = -\frac{543}{322} \quad \alpha_2 = -\frac{188}{205} \tag{8}$$

for NS4PB (Fig. 5b). FE analyses have been carried out with Ansys® version 13 software package. Parabolic isoparametric elements (PLANE183 in ANSYS) have been used with a very fine mesh pattern close to the crack tip, in order to get results with high degree of accuracy.

4. Experimental results

4.1. Tensile tests

The effects of the weight content of Cloisite 30B® nano-additives upon the nanocomposite elastic modulus, strength and strain to failure are reported in Table 3 and summarised in Fig. 6.

The elastic modulus is only slightly affected by nano-additives with improvement up to 8.5% for a 5 wt% of nanoclay content.

Table 3
Tensile properties of neat epoxy and nanomodified polymers.

Nanoclay content (wt%)	E (MPa)	σ_R (MPa)	ε_f (%)	ν
Neat epoxy	3392 ± 16	68.8 ± 4.5	2.72 ± 0.32	0.347 ± 0.003
1	3382 ± 79	68.0 ± 0.9	2.96 ± 0.13	0.377 ± 0.002
3	3599 ± 38	57.5 ± 7.6	2.19 ± 0.32	0.373 ± 0.005
5	3679 ± 116	51.5 ± 4.2	1.66 ± 0.14	0.370 ± 0.006

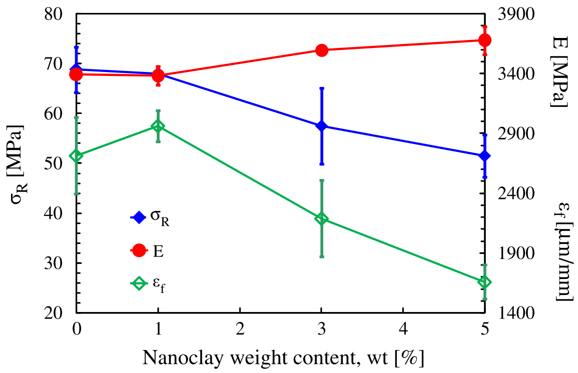

Fig. 6. Results of tensile tests on neat and nanomodified epoxy resins.

Conversely, nanomodification has a detrimental effect in terms of strength and strain to failure.

Indeed the nanocomposite strength is decreased from 68.8 MPa (neat resin) to 51.5 MPa (5 wt% nanoclay) with a reduction of about 25.1%, while the addition of nanoclays leads to an initial improvement of the strain to failure (+10% for 1 wt%) followed by a monotonic reduction (−39% for 5 wt%). These results agree with previous findings in the literature [12–15].

It is finally worth mentioning that the limited reduction of the tensile strength due to nanomodification is commonly regarded as non-significant, the improvement of the polymer fracture toughness, shown later, being much more important and interesting [15,16].

4.2. Fracture tests

The force displacement curves of the tests, typified in Fig. 7 for mode I loadings, allow us to conclude that during the tests the material exhibited a pure linear elastic behaviour, the force–displacement plots being linear up to the fracture load.

A summary of all experimental data, expressed in terms of SIFs according to Eq. (3), is shown in Fig. 8.

It is evident that nanomodified specimens exhibit a higher fracture toughness, independently of the loading mode.

The highest improvement was obtained under pure mode I loading conditions, with a maximum increment of 48.7% in terms of K_{IC} for 1 wt% content of nanofiller.

Ranging from pure mode I to pure mode II less pronounced improvements can be noted. Under pure mode II loading conditions the higher fracture toughness is exhibited by specimens loaded with 1 wt% content of nanofiller (+24.1%).

4.3. Crack paths

Some pictures of fractured specimens with 1 wt% of nanoclay are shown in Fig. 9. Mode I loaded specimens fractured along the initial crack plane ($\theta = 0$). Differently, the presence of mode II loadings gives rise to a crack tilting. For specimens under mixed mode loadings with $\phi = 0.3$ (Fig. 9b), the fracture took place at a measured angle θ = 36–38° with respect to the

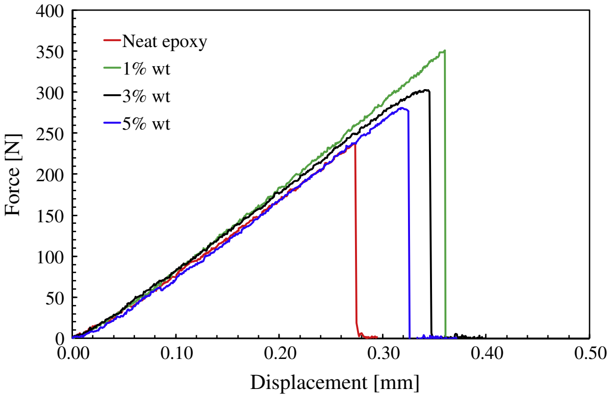

Fig. 7. Force–displacement diagrams for neat epoxy and nanomodified specimens under mode I loading.

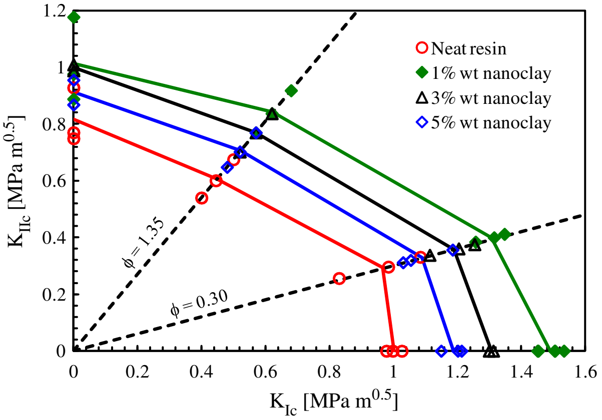

Fig. 8. Fracture toughness of neat and nanomodified specimens under various loading conditions.

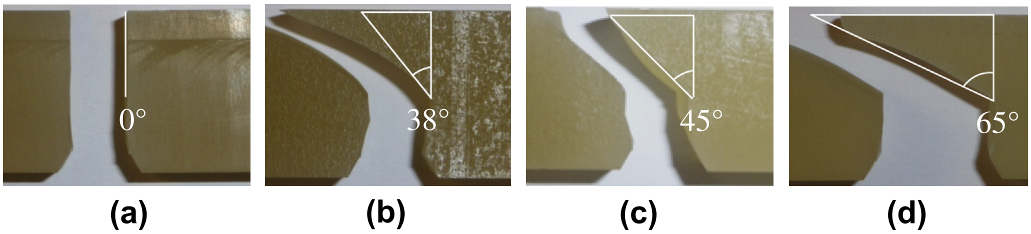

Fig. 9. Fracture angles for (a) mode I, (b) mixed mode $K_{II}/K_I = 0.30$, (c) mixed mode $K_{II}/K_I = 1.35$ and (d) mode II loading conditions. Specimens with 1 wt% of nanoclay.

crack line. For $\phi = 1.35$ (Fig. 9c), $\theta = 44–45°$ while for mode II loaded specimens (Fig. 9d) the crack tilted at about 63–65°. No clear effect of nanomodification was noted on the crack initiation angle.

4.4. Morphological analysis of the fracture surfaces

In order to better understand the mechanical behaviour of the nanocomposite systems at different loading conditions, a morphological analysis of the fracture surfaces was carried out by means of a Quanta400 scanning electron microscope produced by FEI.

The fracture surfaces of the neat epoxy, taken from a region close to the initial crack front, are shown in Fig. 10, where the arrows indicate the direction of crack propagation. It is evident that, except for some river line markings near the crack initiation site, the fracture surfaces appeared to be very smooth, independently of the investigated loading condition. Such a morphology is typical of brittle polymers.

On the other hand, for all the analysed loading conditions, the fracture surfaces of nanomodified specimens were found very rough. An example from 5 wt% nanomodified specimens is shown in Fig. 11. All pictures have been taken from a region close to the initial crack front and the arrows indicate the direction of crack propagation. Under pure mode I loading (Fig. 11a), the emergence of many steps throughout the whole surface can be noted. This morphology is commonly

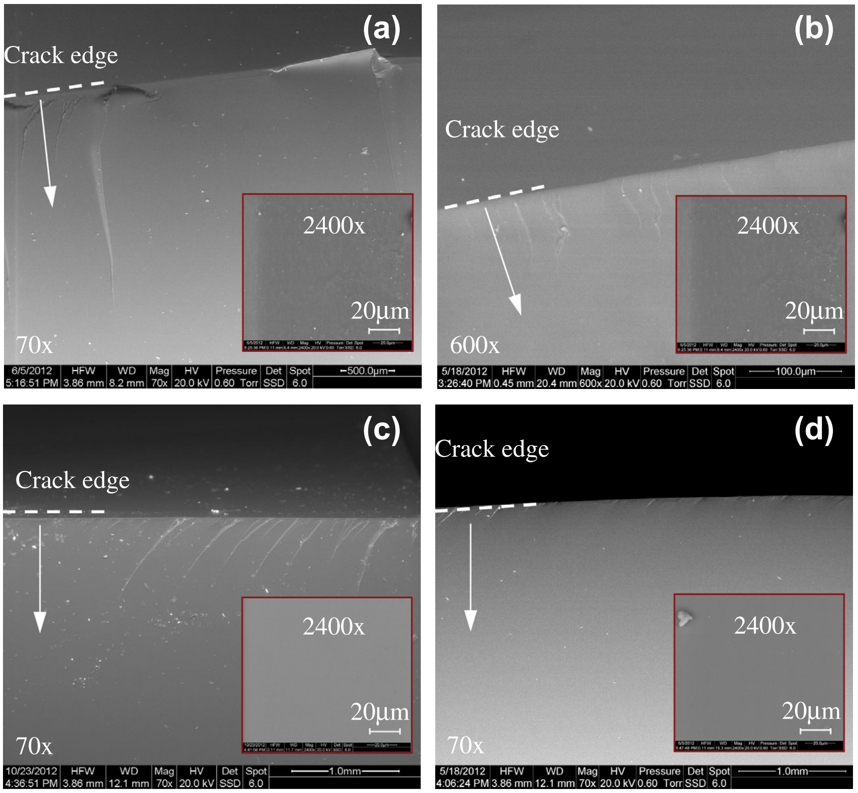

Fig. 10. SEM micrographs of fracture surfaces for neat epoxy. Pure mode I (a), $\phi = 0.30$ (b), $\phi = 1.35$ (c), pure mode II (d).

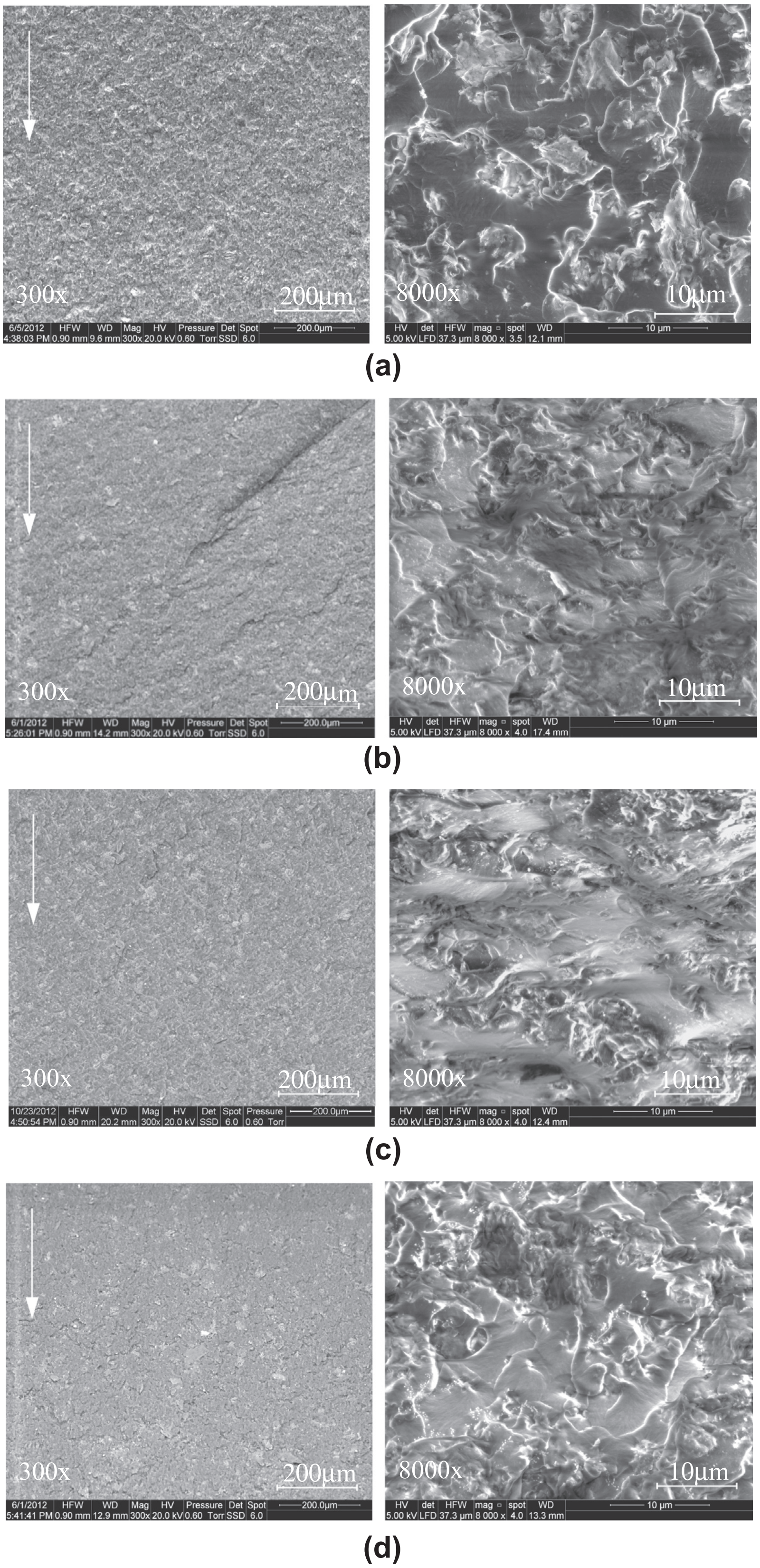

Fig. 11. SEM micrographs of fractue surfaces for 5 wt% nanocomposite. Pure mode I (a), $\phi = 0.30$ (b), $\phi = 1.35$ (c), Pure mode II (d).

acknowledged to be due to secondary crack fronts divided by aggregates and it denotes that microcracking and subsequent microcrack coalescence in different planes have taken place.

These phenomena, which are reasonably due to the presence of nanoclays in the epoxy resin, are the main detected toughening mechanism, which can be regarded as responsible of fracture toughness improvements exhibited by nanoclay loaded specimens. It is worth mentioning that a similar morphology was observed also by Wang et al. [14] for a Epoxy/Cloisite 93A system.

Fig. 11b–d document that the step area density depend on the loading mode. Indeed, higher magnification images show that, even if the toughening mechanism is the same, its extent within the process zone reduces while moving from pure mode I to pure mode II. This is compliant with experimental results discussed in Section 4.2, according to which the fracture toughness improvement due to nanomodification is dependent on the loading mode, being higher under pure mode I loadings.

It is worth finally mentioning that similar morphologies were observed also in nanomodified specimens with different clay contents.

5. Prediction of mixed mode fracture behaviour of nanocomposites

In the past and recent literature several theoretical or empirical criteria for mixed mode fracture for brittle homogeneous materials have been proposed and validated (see, amongst the others, [25–31]). Depending on the nature of the criterion, in addition to the critical conditions required for the fracture onset, predictions for the angle of fracture initiation can be also obtained.

However it is recognised that nanocomposite fracture toughness strictly depends on the amount of energy dissipated by the damaging mechanisms taking place at the nanoscale, which are responsible for material toughening [32–36]. Moreover the toughness improvements associated with nanomodification are strongly influenced by many factors, such as the filler morphology (size, geometry and distribution) and, in particular, the applied loading conditions. Accordingly additional inherent difficulties are expected while modelling the mixed mode fracture behaviour of this kind of new materials.

In the following sections a brief overview of three mixed mode fracture criteria widely used in the literature, i.e. the MTS criterion [25], the S criterion [26] and Richard's criterion [30,31] is provided. Then, with the main aim to identify a mixed mode criterion providing reliable predictions for nanomodified polymers, a comparison is carried out with the experimental results obtained in the present work.

5.1. Maximum Tangential Stress Criterion (MTS criterion)

The Maximum Tangential Stress criterion (MTS) [25] assumes that the crack propagation is controlled by the maximum value of the hoop stress at the crack tip, $\sigma_{\theta\theta,\max}$. In particular, the fracture initiation angle equates the direction of $\sigma_{\theta\theta,\max}$ [25]:

$$\theta_0 = -\arccos\left(\frac{3\phi^2 + \sqrt{1+8\phi^2}}{1+9\phi^2}\right) \tag{9}$$

The general condition for the crack onset can instead be written as [25]:

$$K_{\mathrm{I}}\left[\cos\frac{\theta_0}{2}\left(\cos^2\frac{\theta_0}{2} - \frac{3}{2}\phi\sin\theta_0\right)\right] = K_{\mathrm{Ic}} \tag{10}$$

5.2. Minimum strain energy density criterion (S criterion)

The S criterion [26] states that brittle fracture is controlled by the strain energy density factor S, which, under mixed mode (I + II) assumes the following quadratic form:

$$S = a_{11}K_{\mathrm{I}}^2 + 2\,a_{12}K_{\mathrm{I}}K_{\mathrm{II}} + a_{22}K_{\mathrm{II}}^2 \tag{11}$$

where

$$\begin{aligned} a_{11} &= \frac{1}{16\pi\mu}[(1+\cos\ \theta)(\kappa-\cos\ \theta)] \\ a_{12} &= \frac{1}{16\pi\mu}\sin\theta[2\cos\ \theta-(\kappa-1)] \\ a_{22} &= \frac{1}{16\pi\mu}[(\kappa+1)(1-\cos\ \theta)+(1+\cos\theta)(3\cos\ \theta-1)] \end{aligned} \tag{12a, b, c}$$

being μ the shear modulus and, for plane strain conditions, $\kappa = 3 - 4\nu$.

The initial crack growth is assumed to take place in the direction along which the S factor has a stationary (minimum) value [26]:

$$\left.\frac{\partial S}{\partial \theta}\right|_{\theta=\theta_0} = 0 \tag{13}$$

or, in more explicit form:

$$4\phi \cos 2\theta_0 + \lfloor (\kappa+1) + (\kappa-1)\phi^2 \rfloor \sin\theta_0 - 2\cos\theta_0 \lfloor (\kappa-1)\phi + (1+3\phi^2)\sin\theta_0 \rfloor = 0 \tag{14}$$

It is also supposed that crack initiation occurs when the S factor reaches a critical value, i.e. $S = S_{cr}$. This last condition gives the following fracture locus:

$$\begin{aligned} K_\mathrm{I} = K_\mathrm{Ic}\Bigg\{\frac{8}{\kappa-1}\Bigg[&\frac{1}{16}(1+\cos\theta_0)(\kappa-\cos\theta_0) + \frac{1}{8}\sin\theta_0(2\cos\theta_0-(\kappa-1))\phi + \frac{1}{16}((\kappa+1)(1-\cos\theta_0) \\ &+(1+\cos\theta_0)(3\cos\theta_0-1))\phi^2\Bigg]\Bigg\}^{-0.5} \end{aligned} \tag{15}$$

5.3. Richard's criterion

According to Richard's criterion [30,31], the mixed mode fracture locus is described by the following equation:

$$\frac{K_\mathrm{I}}{K_\mathrm{Ic}} + \frac{K_\mathrm{II}^2}{K_\mathrm{IIc}^2} = 1 \tag{16}$$

where K_Ic and K_IIc are the pure mode I and pure mode II fracture toughness, respectively.

Eq. (16) can be equivalently rewritten as follows:

$$K_\mathrm{I} = K_\mathrm{Ic}\left[1 - \left(\frac{K_\mathrm{II}}{K_\mathrm{IIc}}\right)^2\right] \tag{17}$$

As a major experimental drawback with respect to the previous ones, Richard's criterion requires fracture toughness under pure mode I, K_Ic, and pure mode II, K_IIc, to be known. On the other hand it can probably capture the difference in the material response due to the mode of loading.

Table 4
Comparison between the fracture angles measured from experiments and the predicted values using the MTS and the S criterions ($\nu = 0.37$).

ϕ	θ_0, Experiments (°)	θ_0, MTS criterion (°)	θ_0, S criterion (°)
0	0	0	0
0.3	−38	−29	−33
1.35	−45	−57	−57
∞	−65	−70	−85

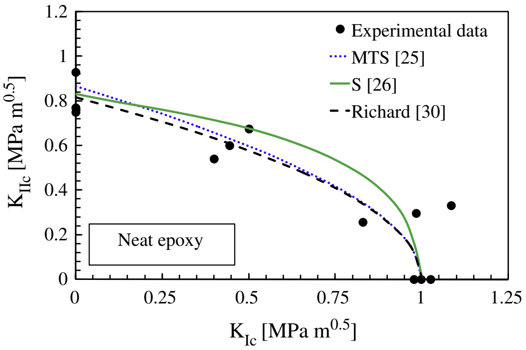

Fig. 12. Comparison between predicted fracture toughness values and experimental results. Cracked specimens made of neat epoxy.

5.4. Discussion

A satisfactory agreement was found between the fracture angles measured from experiments and the predicted values using the MTS and the S criterions (see Table 4).

Moreover, the predictions based on the mixed mode fracture toughness criteria discussed in the previous sections have been compared with the experimental data obtained in the present work. The comparison is shown in Figs. 12–15 for different nanoclay contents.

Fig. 12 shows that the results from specimens made of pure epoxy are well predicted by almost all the fracture criteria before mentioned.

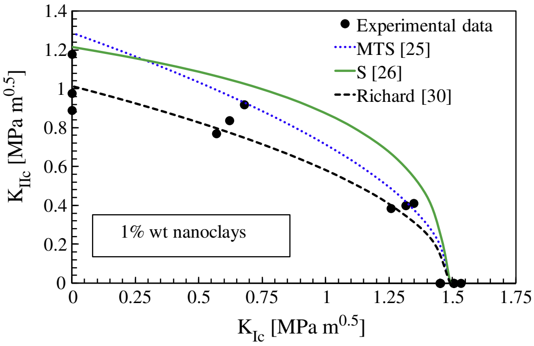

Fig. 13. Comparison between predicted fracture toughness values and experimental results. Cracked specimens made of epoxy resin filled with 1 wt% of nanoclays.

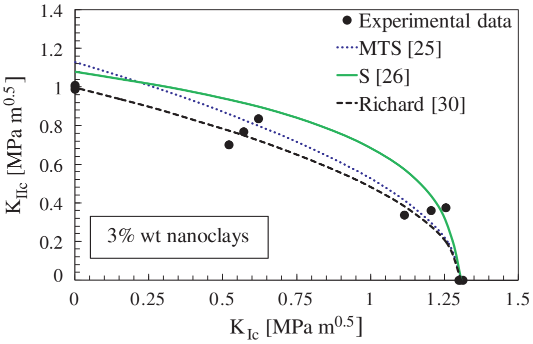

Fig. 14. Comparison between predicted fracture toughness values and experimental results. Cracked specimens made of epoxy resin filled with 3 wt% of nanoclays.

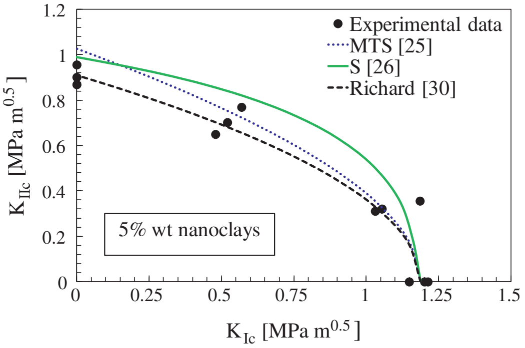

Fig. 15. Comparison between predicted fracture toughness values and experimental results. Cracked specimens made of epoxy resin filled with 5 wt% of nanoclays.

Differently, in the case of nanomodified specimens, the accuracy of the fracture criteria based only on K_{Ic} is poorer and the best prediction of mixed mode fracture toughness is provided by Richard's criterion (see Figs. 13–15).

The inaccuracy of classical mixed mode fracture criteria, MTS and S, for results from nanomodified polymers can be due to the emergence of different damaging mechanisms taking place at the microscale and nanoscale which can be influenced by the loading mode, as discussed in Section 4.4.

Richard's criterion, instead, is capable of better predictions since it is based either on K_{IC} or on K_{IIC}, thus accounting, in some way, for the change of material damaging moving from pure mode I to pure mode II.

6. Conclusion

In the present work the effects of nanoclay addition on the fracture behaviour of an epoxy resin under mixed mode (I + II) loadings have been studied by analysing the results from Single Edge Notch Bending (SENB) tests. The results allow to conclude that, for weight contents up to 5 wt%, nanomodification significantly enhances the fracture toughness of the epoxy resin upon the entire range of mixed mode loadings, the improvements being dependent on the mode mixity ratio.

Experimental results have been compared to the theoretical predictions based on three mixed mode fracture criteria for brittle homogeneous solids. The results from specimens made of pure epoxy are well predicted, almost independently of the approach used for the synthesis. Conversely, as far as the results from specimens made of nanomodified polymer are concerned, the agreement with theoretical predictions by one-parametrical approaches is worse. This can be thought of as linked to the emergence, due to nanomodification, of different damaging mechanisms depending on the mode mixity.

Better predictions were obtained using Richard's criterion.

Acknowledgements

The authors greatly acknowledge the financial support to the activity by Veneto Nanotech, the Italian Cluster on Nanotechnologies. The authors wish also to thank Dr. Alberto Fabrizi for his support in carrying out the SEM analyses.

References

[1] Fischer H. Polymer nanocomposites: from fundamental research to specific applications. Mater Sci Engng C 2003;23:763–72.
[2] Thostenson ET, Li C, Chou TW. Nanocomposites in context. Compos Sci Technol 2005;65:491–516.
[3] Ajayan PM, Schadler LS, Braun PV. Nanocomposite science and technology. Wiley-VCH; 2003, ISBN 3527303596.
[4] Zappalorto M, Salviato M, Quaresimin M. Assessment of debonding-induced toughening in nanocomposites. Procedia Engng 2011;10:2973–8.
[5] Salviato M, Zappalorto M, Quaresimin M. Plastic yielding around nanovoids. Procedia Engng 2011;10:3316–21.
[6] Zappalorto M, Salviato M, Quaresimin M. Influence of the interphase zone on the nanoparticle debonding stress. Compos Sci Technol 2011;72:48–55.
[7] Salviato M, Zappalorto M, Quaresimin M. The effect of surface stresses on the critical debonding stress around nanoparticles. Int J Fract 2011;172:97–103.
[8] Cho JW, Paul DR. Nylon 6 nanocomposites by melt compounding. Polymer 2001;42:1083–94.
[9] Wang L, Wang K, Chen L, Zhang Y, He C. Preparation, morphology and thermal/mechanical properties of epoxy/nanoclay composite. Compos Part A – Appl S 2006;37:1890–6.
[10] Liu TX, Liu ZH, Ma KX, Shen L, Zeng KY, He CB. Morphology, thermal and mechanical behavior of polyamide 6/layered-silicate nanocomposites. Compos Sci Technol 2003;63:331–7.
[11] Lee DC, Jang LW. Preparation and characterization of PMMA-clay hybrid composite by emulsion polymerization. J Appl Polym Sci 1996;61:1117–22.
[12] Luo J, Daniel IM. Characterization and modeling of mechanical behavior of polymer/clay nanocomposites. Compos Sci Technol 2003;63:1607–16.
[13] Bharadwaj RK, Mehrabi AR, Hamilton C, Trujillo C, Murgaa M, Fan R, et al. Structure–property relationships in cross-linked polyester–clay nanocomposites. Polymer 2002;43:3699–705.
[14] Wang K, Chen L, Wu J, Toh ML, He C, Yee AF. Epoxy nanocomposites with highly exfoliated clay: mechanical properties and fracture mechanisms. Macromolecules 2005;38:788–800.
[15] Quaresimin M, Salviato M, Zappalorto M. Fracture and interlaminar properties of clay-modified epoxies and their glass reinforced laminates. Engng Fract Mech 2012;81:80–93.
[16] Quaresimin M, Salviato M, Zappalorto M. Strategies for the assessment of nanocomposite mechanical properties. Compos Part B – Engng 2012;43:2290–7.
[17] Subramaniyan AK, Sun CT. Toughening polymeric composites using nanoclay: crack tip scale effects on fracture toughness. Compos Part A – Appl S 2007;38:34–43.
[18] Becker O, Varley R, Simona G. Morphology, thermal relaxations and mechanical properties of layered silicate nanocomposites based upon high-functionality epoxy resins. Polymer 2002;43:4365–73.
[19] Weon JI, Sue HJ. Effects of clay orientation and aspect ratio on mechanical behaviour of nylon-6 nanocomposite. Polymer 2005;46:6325–34.
[20] Liu W, Hoa SV, Pugh M. Fracture toughness and water uptake of high-performance epoxy/nanoclay nanocomposites. Compos Sci Technol 2005;65:2364–73.
[21] Zerda AS, Lesser AJ. Intercalated clay nanocomposites: morphology, mechanics, and fracture behavior. J Polym Sci Pol Phys 2001;39:1137–46.
[22] Kornman X, Thomann R, Mulhaupt R, Finter J, Berglund LA. High performance epoxy-layered silicate nanocomposites. Polym Engng Sci 2002;42:1815–26.
[23] Ayatollahi MR, Shadlou S, Shokrieh MM. Mixed mode brittle fracture in epoxy/multi-walled carbon nanotube nanocomposites. Engng Fract Mech 2011;78:2620–32.
[24] ASTM D 5045, Standard test methods for plane-strain fracture toughness and strain energy release rate of plastic materials; 1999.
[25] Erdogan F, Sih GC. On the crack extension in plates under plane loading and transverse shear. Trans ASME, J Basic Engng 1963;85:519–27.
[26] Sih GC. Strain-energy-density factor applied to mixed mode crack problems. Int J Fract 1974;10:305–21.
[27] Hussain MA, Pu SL, Underwood J. Strain energy release rate for a crack under combined mode I and mode II. Fracture analysis. Philadelphia: ASTM STP 560 American Society for Testing and Materials; 1974.
[28] Lazzarin P, Zambardi R. A finite-volume-energy based approach to predict the static and fatigue behaviour of components with sharp V-shaped notches. Int J Fract 2001;112:275–98.
[29] Yosibash Z, Priel E, Leguillon D. A failure criterion for brittle elastic materials under mixed-mode loading. Int J Fract 2006;141:291–312.

[30] Richard HA, Fulland M, Sander M. Theoretical crack path prediction. Fatigue Fract Engng Mater Struct 2005;28:3–12.

[31] Araki W, Nemoto K, Adachi T, Yamaji A. Fracture toughness for mixed mode I/II of epoxy resin. Acta Mater 2005;53:869–75.

[32] Hsieh TH, Kinloch AJ, Masania K, Taylor AC, Sprenger S. The mechanisms and mechanics of the toughening of epoxy polymers modified with silica nanoparticles. Polymer 2010;51:6284–94.

[33] Johnsen BB, Kinloch AJ, Mohammaed RD, Taylor AC, Sprenger S. Toughening mechanisms of nanoparticle-modified epoxy polymers. Polymer 2007;48:530–41.

[34] Lauke B. On the effect of particle size on fracture toughness of polymer composites. Compos Sci Technol 2008;68:3365–72.

[35] Williams JG. Particle toughening of polymers by plastic void growth. Compos Sci Technol 2010;70:885–91.

[36] Zappalorto M, Salviato M, Quaresimin M. A multiscale model to describe nanocomposite fracture toughness enhancement by the plastic yielding of nanovoids. Compos Sci Technol 2012;72:1683–91.